Porphyrin-based porous polymers for CO_2 capture and conversion

Grace Eder

The single largest challenge currently facing humanity is the task of addressing the causes and effects of human-influenced climate change. Unchecked greenhouse gas emissions from burning fossil fuels over decades has drastically changed earth's climate. Among greenhouse gasses, carbon dioxide (CO_2) is known to be one of the major contributors to climate change. Methods to address the abundance of CO_2 in the atmosphere are not only essential to beginning to tackle climate change, but they also provide a significant economical motivation to address this problem; the reduction of CO_2 to common C1 commodity chemicals such as methanol or formic acid have strong potential to form the basis for new energy systems that can be independent of fossil fuels. In particular, formic acid is a target of considerable interest because it has several advantages over methanol. Primary among these, it only requires a single reduction of CO_2 to form- whereas further reduction of formic acid is required to obtain methanol. Formic acid also has a lower toxicity and is acknowledged as less environmentally hazardous than methanol. Formic acid can be used as fuel in a number of ways including as a feedstock for the production of hydrogen gas[1] or in a direct formic acid fuel cell.[2] This dual environmental and economic motivation has pushed us to design a catalyst for reduction of CO_2 to formic acid that can be effective and reusable.

A number of catalysts have been developed to reduce CO_2 to formic acid and related derivatives using a hydride source and variety of metals, including ruthenium,[3,4] iridium,[5] nickel,[6] rhodium,[7] zinc,[8] and copper.[9,10] It has also been completed by direct hydrogenation of CO_2 with hydrogen gas[11] and by metal-free catalytic systems.[12,13] With many of these systems, the number of additives, high-pressured gasses, and low potential for recyclability hinder their success. Porous materials that can act as catalysts for the reduction of CO_2 have great potential for success due to their excellent track record of uptake and storage of CO_2,[14–19] and their porous nature allows them to host a catalytic site that can be easily recycled for further use due to its heterogeneous nature.[20–22]

Our catalyst design centers around a porphyrin as an excellent catalyst in a wide variety of reactions.[23–25] Porphryins have also been used quite extensively in porous polymers for catalysis,[26–28] including CO_2 conversion. A variety of metals have been shown to catalyse the conversion of CO_2 into cyclic carbonates.[29] Another excellent example by the Yaghi group turned a Co-porphyrin COF into a catalyst for the electrochemical reduction of CO_2 to carbon monoxide (CO).[30] While these examples have good value in their proof of principle, they do not directly produce useful compounds for the fuel industry. Our interest was captured by the reduction of CO_2 by silanes to create silyl formates. Silyl formates these have the double utility of being synthetically useful reactive intermediates in organic chemical synthesis and are easily converted to formic acid or a salt thereof for potential fuel applications. Silanes are relatively inexpensive and easy to

handle materials compared to epoxides, which are required for the formation of cyclic carbonates. The hydrosilation of CO_2 by a porous polymer catalyst also has the benefit of simple wet chemistry setup compared to the electrode fabrication and cell set-up required for electrochemical reductions.

Polymer Design and Synthesis

Our catalyst design takes advantage of the simplicity of this reaction using a porphyrin as the catalytic site, and improves on some of the existing porous polymer catalysts by incorporating oxazole and thiazole linkages, which have shown to promote CO_2 uptake in the bulk material and have excellent stability to water. Herein we report 4 novel porous polymers based on porphyrins for catalysis of hydrosilation of CO_2. The monomeric oxazole salt **2**,[16] thiazole salt **3**,[31] and formyl porphyrin **1**[32] were all prepared by modified literature procedures (see Scheme 1). Oxazole porphryin polymers were created by solvothermal synthesis in DMF by a previously reported procedure,[16] and thiazole porphyrin polymers by a modified version of this procedure. Porphyrin POPs **1A** and **1B** were created with the free base porphyrin **1**, as a baseline against which to compare the metallated polymers. The reaction conditions for the polymers were optimized by screening a variety of conditions including different solvents and catalysts (see Tables 1 and 2).

POPs 1A and 1B were characterized by Fourier transform infrared spectroscopy (FT-IR). The FT-IR spectrum of POPs 1A and 1B display the characteristic C=N stretching of the porphyrin at ~1600 cm^{-1} and the oxazole or thiazole stretch at ~1700 cm^{-1} with significant attenuation of the C=O stretch from monomer **1** and the OH, NH_2, and SH stretches of the salt **2** or **3**, indicating complete conversion to the oxazole or thiazole (see Figures 1 and 2).

The permanent porosity of porphyrin POPs was measured by nitrogen gas adsorption at 77 K (see Figure 3). The porphryin POPs both exhibited reversible type I isotherms with small hysteresis. Application of the Brunauer-Emmett-Teller (BET) model over the low pressure region ($0.001<P/P^{\circ}<0.1$) provided surface areas of 760 m^2/g and 535 m^2/g for the POP 1A and POP 1B respectively. Nonlocal density functional theory (NLDFT) was used to estimate the pore size distribution of the POPs 1A and 1B yielding values of 2.46 nm for both POP 1A and 1B (see Figure 4). The CO_2 uptake capacity of POPs 1A and 1B was measured by CO_2 adsorption isotherms at 295 K from 0 to 1.2 bar (see Figure 5). Both POPs 1A and 2A exhibited respectable CO_2 uptake at low pressures reaching capacities of 1.89 and 1.36 mmol/g for POPs 1A and 1B respectively

Powder X-Ray Diffraction (PXRD) analysis of the porphyrin POPs revealed amorphous materials with no long range order (see Figures 6 and 7). We were surprised to find these materials are completely amorphous, given the large number of porphyrin-based COFs reported in the literature. Additionally, POPs 1A

and 1B were made by the same method which produced crystalline BBO-COF 1 and 2. We hypothesize that the phenyl rings at the meso positions of the porphyrin, which naturally assume a 90˚ angle to the plane of the macrocycle, are prohibiting the material from fully planarizing, resulting in an amorphous material.

Catalytic performance

In order to test the catalytic ability of ruthenium porphyrins in CO_2 reduction by hydrosilation, we synthesized a small molecule homogeneous catalyst (RuTPP) as an analogue to determine the optimal conditions for catalysis (see Figure 8). The catalysis was completed by solvothermal synthesis combining RuTPP and potassium fluoride (KF) in a dry vial. A solution of silane in the desired solvent was added, and the mixture was warmed to the boiling point of the solvent under an atmosphere of CO_2 for the desired reaction time (see Scheme 3). The resulting salt, potassium formate, can be easily isolated as a solid and identified by NMR. A quantitative NMR experiment was performed for each trial to determine the yield of the reaction (see Figure 9). The products of the catalytic reaction were dissolved in D_2O (0.7 mL) and an internal standard, DMSO, was added as a comparison point to quantify the amount of potassium formate created by the integration of the peaks in the ^1H NMR. The results of these trials are summarized in Table 3.

From these preliminary trials, we found that Me_2PhSiH was the most effective silane for this reaction giving an optimized yield of 70% in MeCN. Dioxane was

our initial solvent of choice for this reaction based on a procedure for hydrosilation of CO_2 using a copper catalyst. While the reaction in dioxane did allow for the formation of potassium formate, the yields were prohibitively low, thus other solvents were tested. THF was employed in this reaction for its similarity to dioxane, however it caused worse performance of our catalyst. We believe this to be due to the low boiling point of THF, which required lower reaction temperatures. Finally, MeCN was shown to be the solvent performing the highest in our catalytic system, pushing the yield over 10% without rigorous optimization of the reaction conditions. Further optimization of the catalytic reaction continues in our laboratory.

Since the catalysis trials using RuTPP showed some initial success, we moved on to synthesize the ruthenium-containing porphyrin POPs. The ruthenium containing porphryin (**1-Ru)** is synthesized from **1** using a ruthenium source in DMF at high temperatures (see Scheme 4). The ruthenium-containing porphyrin POPs 2A and 2B were synthesized by the same methods as 1A and 1B respectively. Porphryin POPs 2A and 2B were characterized by Fourier transform infrared spectroscopy (FT-IR) and were found to display similar resonances to the free-base polymers, with the distinct addition of a strong resonance at ~1930 cm^{-1} assignable to the carbonyl moiety axial on the ruthenium atom (see Figures 10 and 11).

The permanent porosity of POPs 2A and 2B was measured by nitrogen gas adsorption at 77 K. The POPs 2A and 2B both exhibited reversible type I

isotherms with small hysteresis (see Figure 12). Application of the Brunauer-Emmett-Teller (BET) model over the low pressure region ($0.001<P/P^{\circ}<0.1$) provided surface areas of 621 m^2/g and 644 m^2/g for the POP 2A and POP 2B respectively. Interestingly, POPs 2A and 2B showed an increase in surface area compared to the non-metallated POPs 1A and 1B. We believe that the carbonyl axial ligand on ruthenium decreases the pi-pi stacking ability of **1-Ru** compared to **1**, and might increase the space between porphyrins in the polymeric material. Nonlocal density functional theory (NLDFT) was used to estimate the pore size distribution of the POPs 2A and 2B yielding values of 3.26 nm for both POP 2A and 2B (see Figure 13). The CO_2 uptake capacity of POPs 2A and 2B was measured by CO_2 adsorption isotherms at 295 K from 0 to 1.2 bar (see Figure 14). Both POPs 1A and 2A exhibited respectable CO_2 uptake at low pressures reaching capacities of 1.68 and 1.54 mmol/g.

Future Directions

The recent synthesis of porphyrin POPs 2A and 2B requires further characterization of these materials, including PXRD and elemental analysis to determine the ruthenium content of these materials. After the full characterization of these materials, we next wanted to tackle employing POPs 2A and 2B as catalysts for this reaction. A preliminary trial of the optimized catalytic conditions using POP 2B as a catalyst showed qualitative conversion of a small amount of CO_2 to formic acid by NMR. Further quantitative studies and optimization of the catalytic reaction conditions continues in our laboratory.

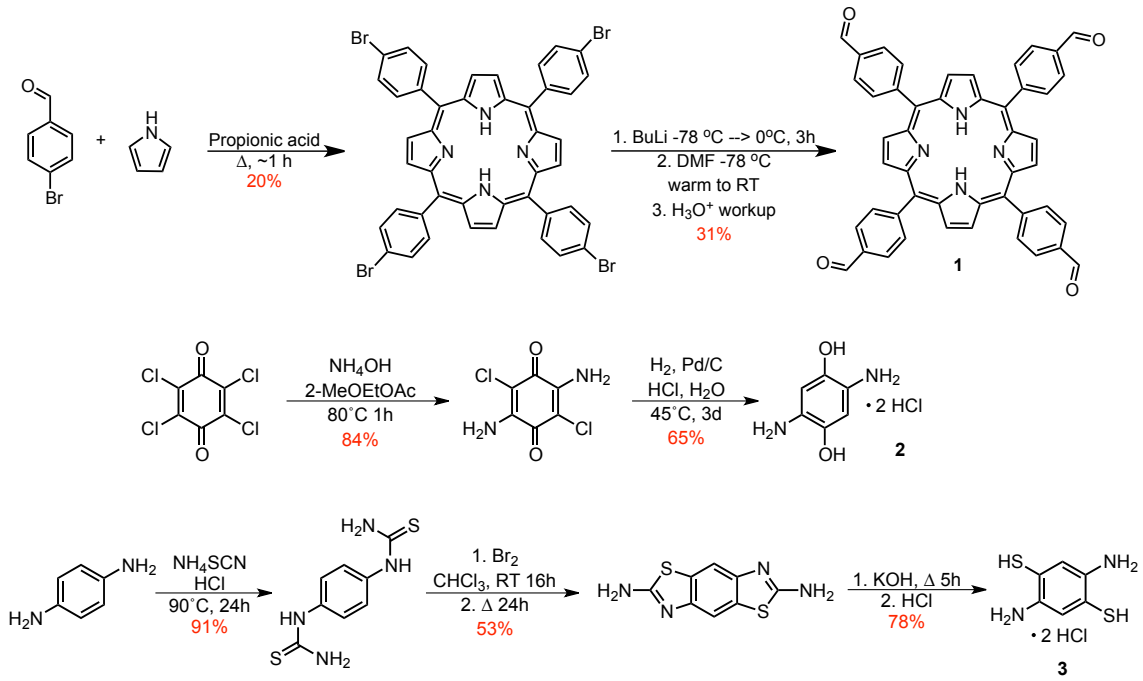

Scheme 1: Synthesis of monomers for porphyrin POPs

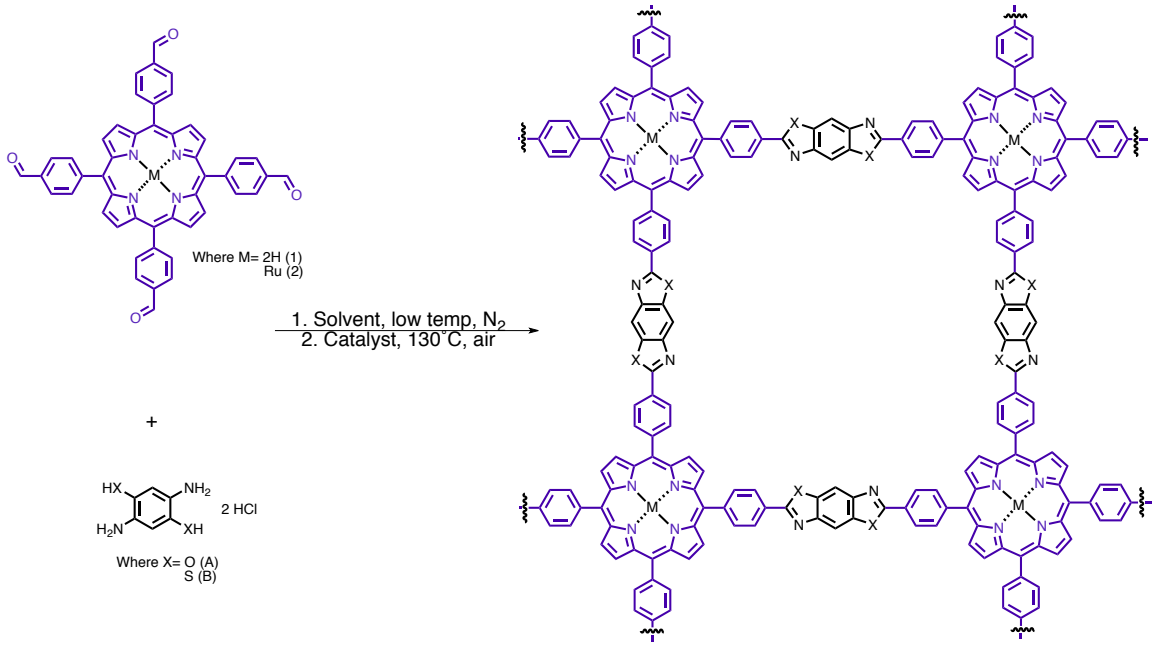

Scheme 2: Synthesis of porphyrin POPs

Oxazole Porphyrin Polymers (1A)			
Trial Set	Condition Changed	Porosity	Pore Size
Eq CN	1 Eq	760 m^2/g	1.46 nm
	0 Eq	566 m^2/g	3.26 nm
Solvents (w/ 1 eq CN)	1:1 DMF: O-xyl	496 m^2/g	1.46 nm
	1:1 DMF: Mes	271 m^2/g	1.46 nm

Table 1: Optimization of reaction conditions for the formation of porphyrin POP 1A

Thiazole Porphyrin Polymers (1B)			
Trial Set	Condition Changed	Porosity	Pore Size
Eq CN	1 Eq	139 m^2/g	1.74 nm
	0 Eq	266 m^2/g	1.46 nm
Solvents (w/ 0 eq CN)	1:1 DMF: O-xyl	535 m^2/g	1.46 nm
	1:1 DMF: Mes	480 m^2/g	1.46 nm

Table 2: Optimization of reaction conditions for the formation of porphyin POP 1B

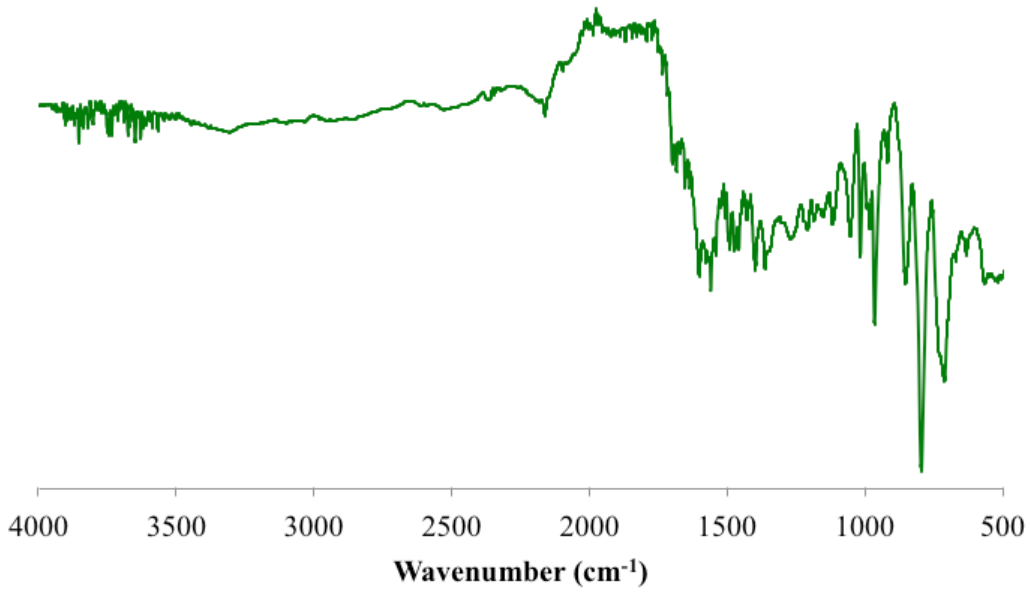

Figure 1: FT-IR spectra of porphyrin POP 1A

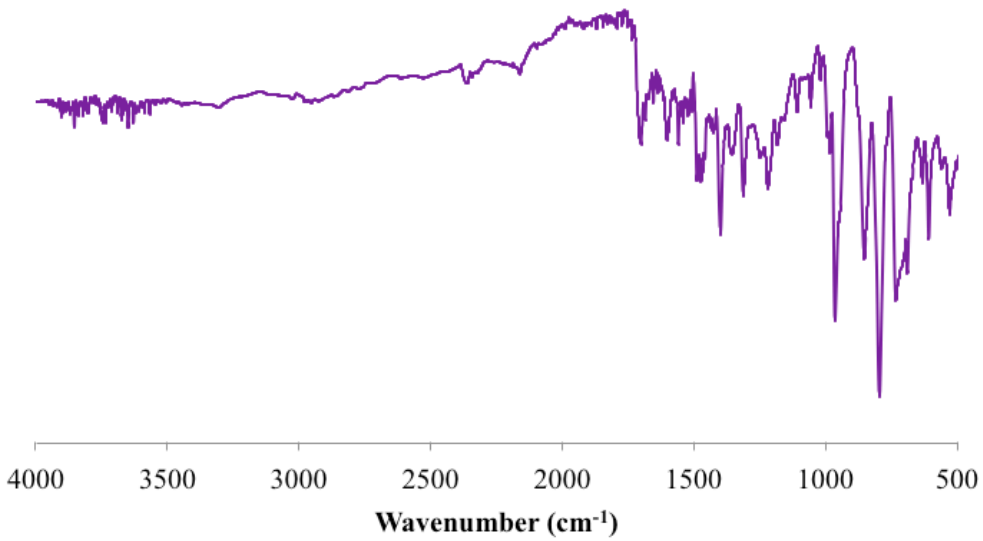

Figure 2: FT-IR spectra of porphyrin POP 1B

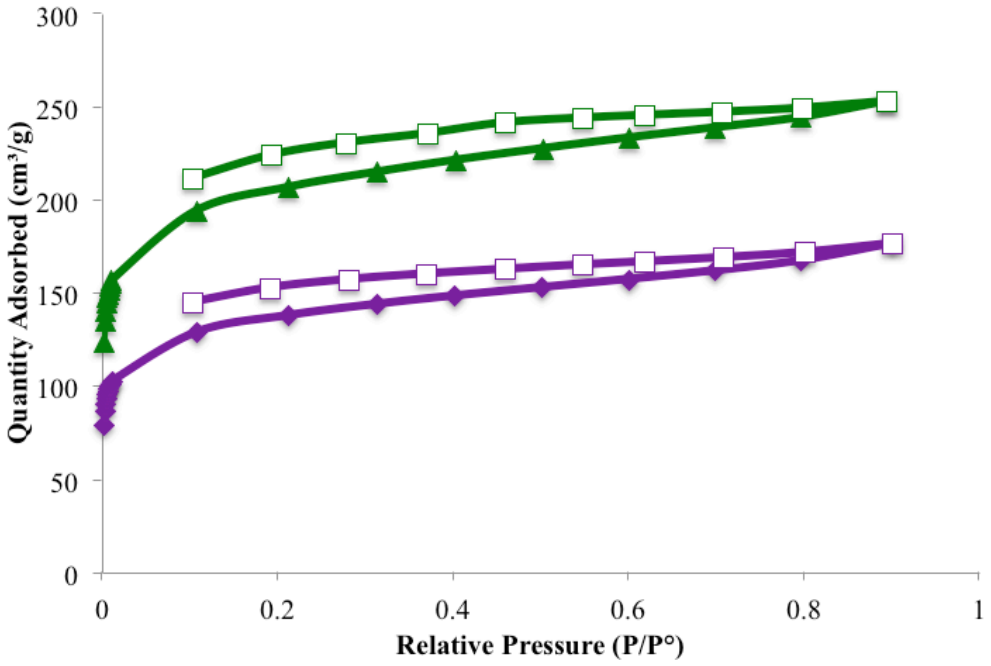

Figure 3: N_2 adsorption isotherms for porphyrin POPs 1A (green) and 1B (purple)

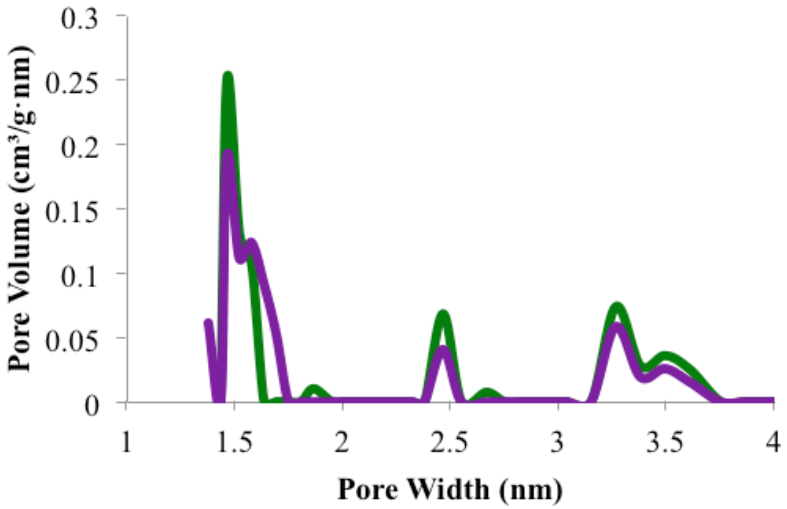

Figure 4: Pore size distribution for porphyrin POPs 1A (green) and 1B (purple)

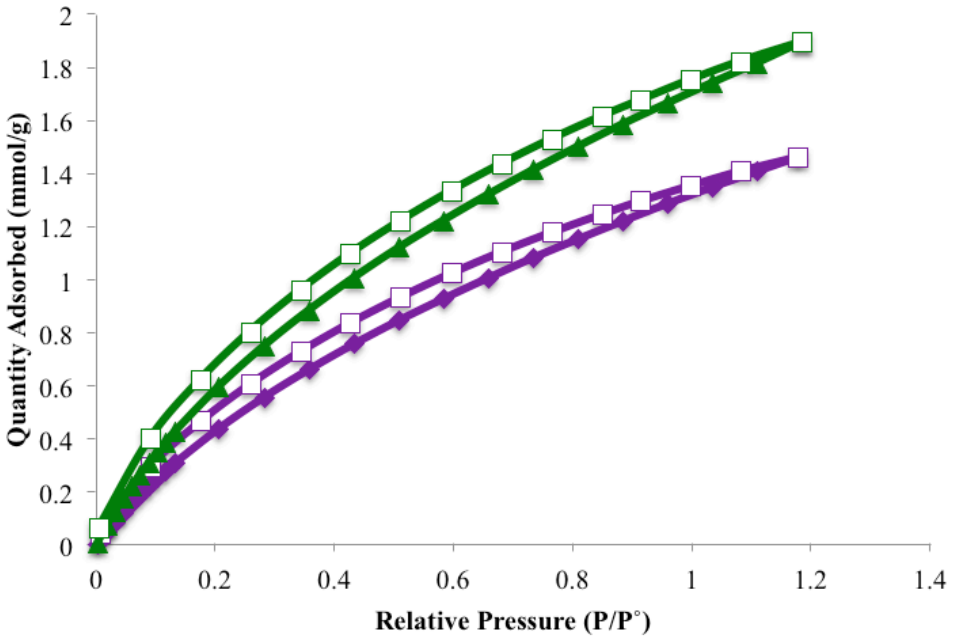

Figure 5: CO_2 adsorption isotherms for porphyrin POPs 1A (green) and 1B (purple)

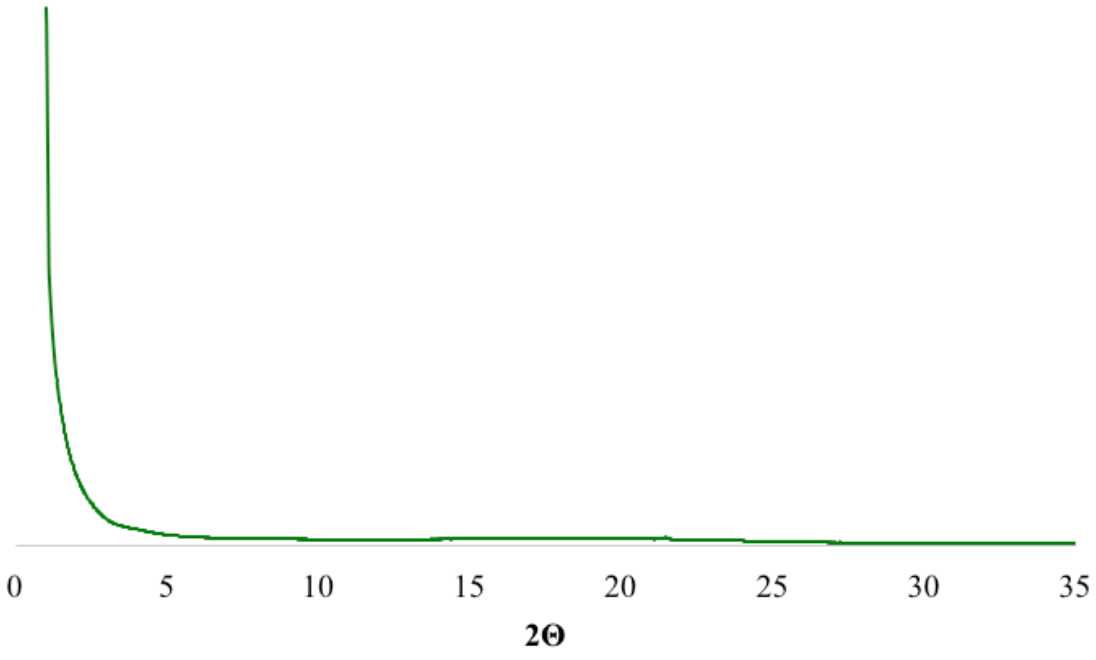

Figure 6: Powder X-Ray diffraction for porphyrin POP 1A

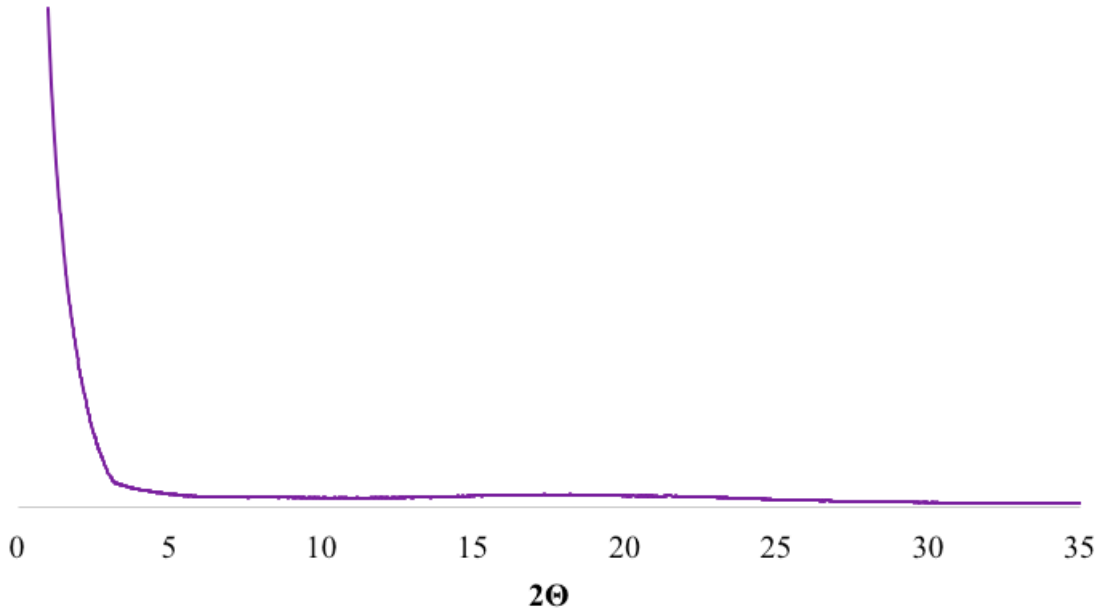

Figure 7: Powder X-Ray diffraction for porphyrin POP 1B

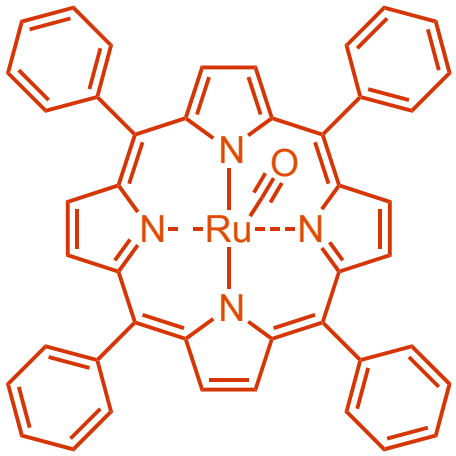

Figure 8: Structure of RuTPP catalyst

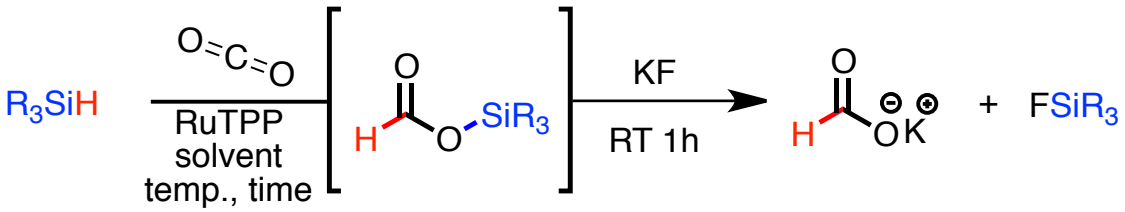

Scheme 3: Synthesis of potassium formate with RuTPP catalyst

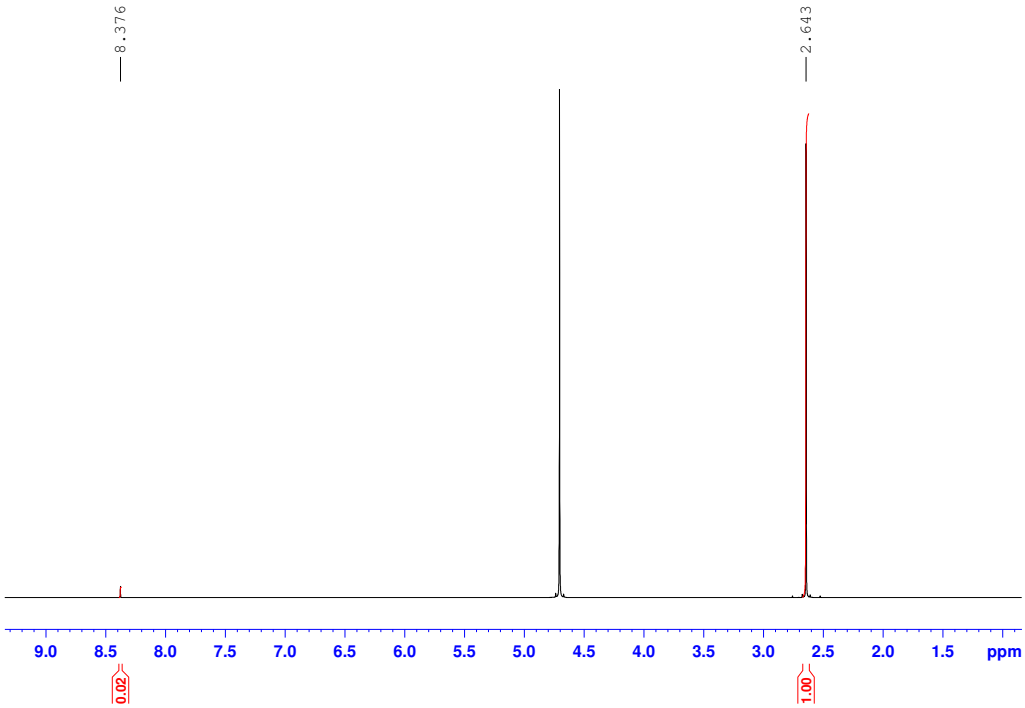

Figure 9: Sample of quantitative NMR spectra for RuTPP catalysis trials. The peak for potassium formate (8.37 ppm) is integrated, and compared against an internal standard, DMSO (2.64 ppm).

Solvent	Reaction Time	Catalyst Loading	Silanes			
			Et_3SiH	PMHS	Me_2PhSiH	$(EtO)_3SiH$
Dioxane	4h	0.5 %	0.01%	0.23%	2.14%	1.49%
	16h	0.5 %	0.32%	0.07%	3.84%	1.88%
	24h	0.5 %	0%	1.09%	4.31%	1.34%
THF	4h	0.5 %	0%	0%	0.63%	0.22%
MeCN	4h	0.5 %	16.4%	1.38%	70.3%	3.95%

Table 3: Summary of hydrosilation of CO_2 trials with RuTPP catalyst

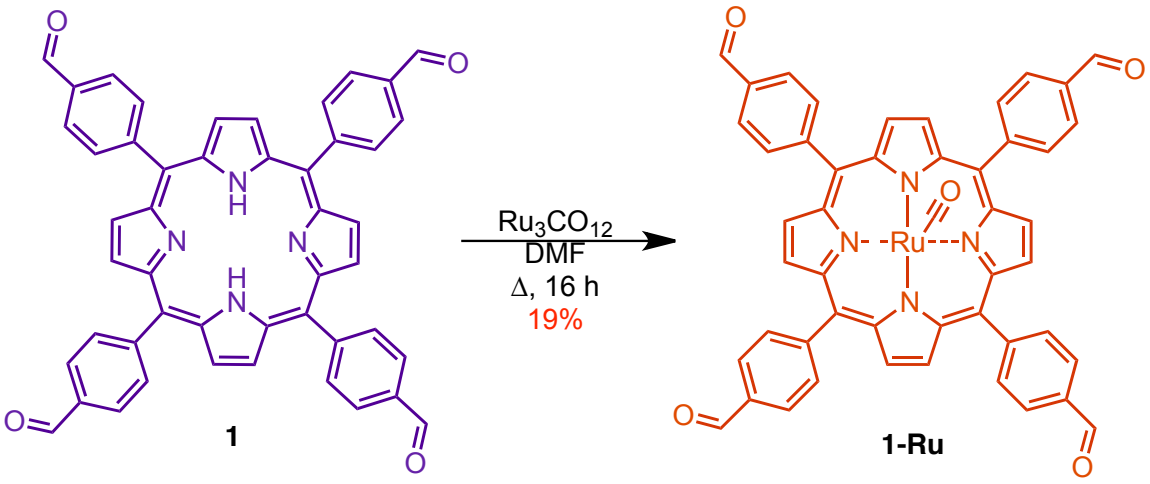

Scheme 4: Synthesis of **1-Ru** from **1**

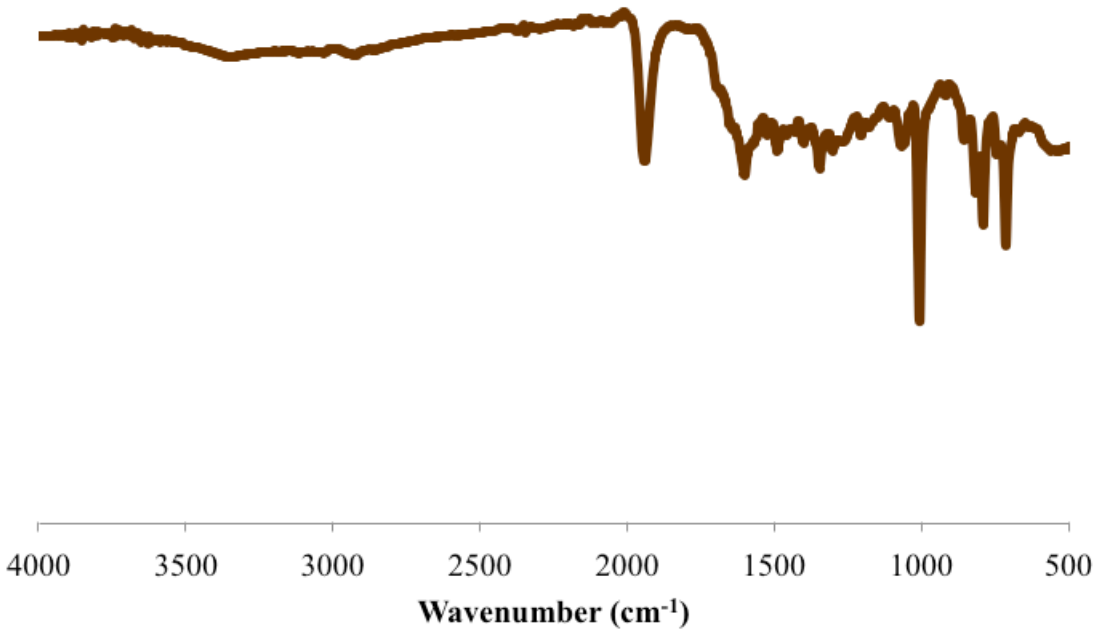

Figure 10: FT-IR spectra of porphyrin POP 2A

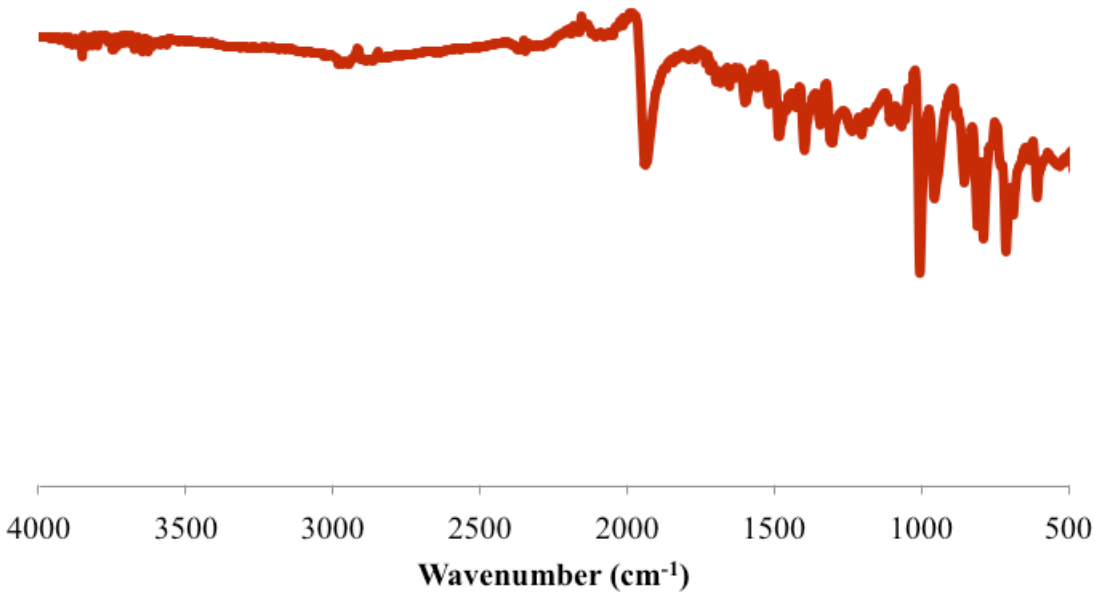

Figure 11: FT-IR spectra for porphryin POP 2B

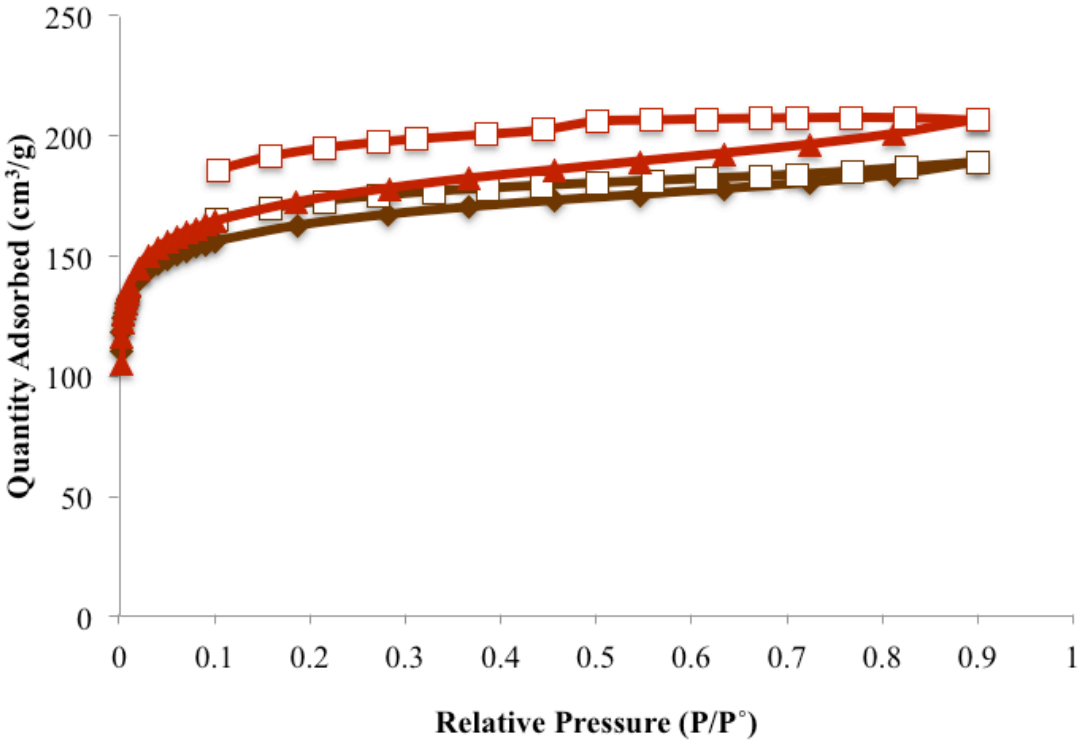

Figure 12: N_2 adsorption isotherms for porphyrin POPs 2A (brown) and 2B (red)

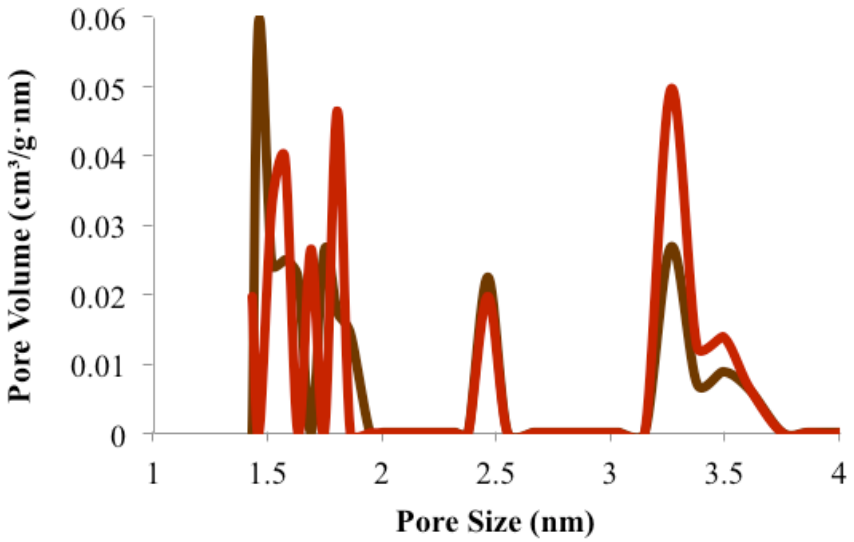

Figure 13: Pore size distribution for porphyrin POPs 2A (brown) and 2B (red)

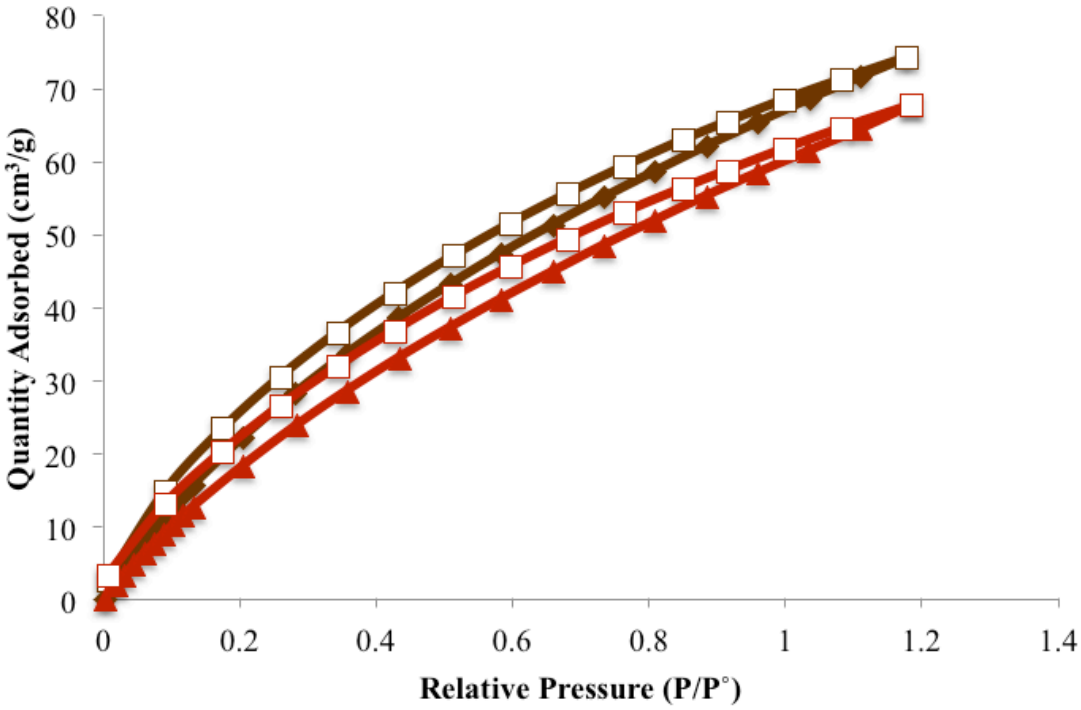

Figure 14: CO_2 adsorption isotherms for porphyrin POPs 2A (brown) and 2B (red)

References:

(1) Eppinger, J.; Huang, K.-W. *ACS Energy Lett.* **2017**, *2*, 188–195.

(2) Yu, X.; Pickup, P. G. *J. Power Sources* **2008**, *182*, 124–132.

(3) Koinuma, H.; Kawakami, F.; Kato, H.; Hirai, H. *J.C.S. Chem. Comm.* **1981**, 213–214.

(4) Jurado-Vázquez, T.; Ortiz-Cervantes, C.; García, J. J. *J. Organomet. Chem.* **2016**, *823*, 8–13.

(5) Oladipo, H. B.; Jaseer, E. A.; Julián, A.; Fernández-Alvarez, F. J.; Al-Khattaf, S.; Oro, L. A. *J. CO2 Util.* **2015**, *12*, 21–26.

(6) González-Sebastián, L.; Flores-Alamo, M.; García, J. J. *Organometallics* **2013**, *32*, 7186–7194.

(7) Itagaki, S.; Yamaguchi, K.; Mizuno, N. *J. Mol. Catal. A Chem.* **2013**, *366*, 347–352.

(8) Sattler, W.; Parkin, G. *J. Am. Chem. Soc.* **2012**, *134*, 17462–17465.

(9) Motokura, K.; Kashiwame, D.; Miyaji, A.; Baba, T. *Org. Lett.* **2012**, *14*, 2642–2645.

(10) Zhang, L.; Cheng, J.; Hou, Z. *Chem. Commun.* **2013**, *49*, 4782.

(11) Moret, S.; Dyson, P. J.; Laurenczy, G. *Nat. Commun.* **2014**, *5*, 1–7.

(12) Schäfer, A.; Saak, W.; Haase, D.; Müller, T. *Angew. Chemie Int. Ed.* **2012**, *51*, 2981–2984.

(13) Mukherjee, D.; Sauer, D. F.; Zanardi, A.; Okuda, J. *Chem. - A Eur. J.* **2016**, *22*, 7730–7733.

(14) Ge, R.; Hao, D.; Shi, Q.; Dong, B.; Leng, W.; Wang, C.; Gao, Y. *J. Chem. Eng. Data* **2016**, *61*, 1904–1909.

(15) Suresh, V. M.; Bonakala, S.; Roy, S.; Balasubramanian, S.; Maji, T. K. *J. Phys* **2014**, *118*, 24369–24376.

(16) Pyles, D. A.; Crowe, J. W.; Baldwin, L. A.; McGrier, P. L. *ACS Macro Lett.* **2016**, *5*, 1055–1058.

(17) Rabbani, M. G.; Islamoglu, T.; El-Kaderi, H. M. *J. Mater. Chem. A* **2017**, *5*, 258–265.

(18) Zhu, X.; Tian, C.; Mahurin, S. M.; Chai, S.-H.; Wang, C.; Brown, S.; Veith, G. M.; Luo, H.; Liu, H.; Dai, S. *J.* **2012**, *134*, 10478–10484.

(19) Xiang, Z.; Mercado, R.; Huck, J. M.; Wang, H.; Guo, Z.; Wang, W.; Cao, D.; Haranczyk, M.; Smit, B. *J. Am. Chem. Soc.* **2015**, *137*, 13301–13307.

(20) Ding, S. Y.; Gao, J.; Wang, Q.; Zhang, Y.; Song, W. G.; Su, C. Y.; Wang, W. *J. Am. Chem. Soc.* **2011**, *133*, 19816–19822.

(21) Buyukcakir, O.; Je, S. H.; Talapaneni, S. N.; Kim, D.; Coskun, A. *ACS Appl. Mater. Interfaces* **2017**, *9*, 7209–7216.

(22) Kim, K.; Kim, S.; Talapaneni, S. N.; Buyukcakir, O.; Almutawa, A. M. I.; Polychronopoulou, K.; Coskun, A. *Polym. (United Kingdom)* **2017**, *126*, 296–302.

(23) Huang, X.; Liu, W.; Hooker, J. M.; Groves, J. T. *Angew. Chemie - Int. Ed.* **2015**, *54*, 5241–5245.

(24) Wang, Y.; Wen, X.; Cui, X.; Wojtas, L.; Zhang, X. P. *J. Am. Chem. Soc.* **2017**, *139*, 1049–1052.

(25) Jiang, X.; Gou, F.; Chen, F.; Jing, H. *Green Chem.* **2016**, *18*, 3567–3576.

(26) Shinde, D. B.; Kandambeth, S.; Pachfule, P.; Kumar, R. R.; Banerjee, R. *Chem. Commun.* **2015**, *51*, 310–313.

(27) Chen, L.; Yang, Y.; Jiang, D. **2010**, 9138–9143.

(28) Shultz, A. M.; Farha, O. K.; Hupp, J. T.; Nguyen, S. T. *Chem. Sci.* **2011**, *2*, 686.

(29) Dai, Z.; Sun, Q.; Liu, X.; Bian, C.; Wu, Q.; Pan, S.; Wang, L.; Meng, X.; Deng, F.; Xiao, F. S. *J. Catal.* **2016**, *338*, 202–209.

(30) Lin, S.; Diercks, C. S.; Zhang, Y.-B.; Kornienko, N.; Nichols, E. M.; Zhao, Y.; Paris, A. R.; Kim, D.; Yang, P.; Yaghi, O. M.; Chang, C. J. *Science* **2015**, *1*, 1–11.

(31) Wolfe, J. F.; Loo, B. H.; Arnold, F. E. *Macromolecules* **1981**, 915–920.

(32) Önal, E.; Ahsen, V.; Pécaut, J.; Luneau, D.; Hirel, C. *Tet. Lett.* **2015**, *56*, 5157–5160.